Available online at www.sciencedirect.com
SCIENCE DIRECT®
Optics Communications 251 (2005) 306–314
OPTICS COMMUNICATIONS
www.elsevier.com/locate/optcom

Spiral phase elements obtained by use of discrete space-variant subwavelength gratings

Avi Niv *, Gabriel Biener, Vladimir Kleiner, Erez Hasman

Optical Engineering Laboratory, Faculty of Mechanical Engineering, Technion-Israel Institute of Technology, Haifa 32000, Israel

Received 3 January 2005; received in revised form 1 March 2005; accepted 2 March 2005

Abstract

The formation of spiral phase elements producing helical beams with different topological charges is presented. The elements consist of discrete space-variant subwavelength dielectric gratings. We demonstrate our approach by fabricating elements for circularly polarized laser radiation with a wavelength of 10.6 μm. The resulting helical phases, as well as the birefrigent parameters of the element, are measured by analyzing the polarization-dependency of the elements along with the self-interference characteristics of the emerging beams.

Keywords: Helical phase; Spiral element; Subwavelength grating; Space-variant grating; Singular optics; Optical vortex

1. Introduction

Spiral phase elements are optical components that produce beams with a helical phase distribution. Such beams are characterized by a complex amplitude of the form: $u(r,\omega) \propto \exp(il\omega)$, where r and ω are the radii and azimuth of the polar coordinates, respectively, and l is the topological charge of the beam. Helical beams have attracted much interest of late, both in theoretical and applied terms. This is mainly due to their dark central core and the ability to transfer angular momentum [1]. For example, helical beams have been used in optical tweezers for trapping and transferring angular momentum to microscopic particles [2–5]. Helical beams have also found applications in optical transformations [6], frequency shifting [7], and the study of optical vortices [8]. The formation of helical beams can be achieved by means of computer-generated holograms [1,2,6,8], programmable liquid crystal displays [9] and refractive spiral phase elements [10]. Helical beams can also be formed by the insertion of a spiral phase element directly into a laser cavity [11]. However, all these methods are either cumbersome or have low efficiency.

* Corresponding author. Tel.: +97248292151; fax: +97248295711.
E-mail address: navi@tx.technion.ac.il (A. Niv).

0030-4018/$ - see front matter © 2005 Elsevier B.V. All rights reserved.
doi:10.1016/j.optcom.2005.03.002

Previously, we had demonstrated the formation of helical beams with various topological charges based on the geometrical Pancharatnam phase [12]. In this case, the phase, which resulted directly from polarization state manipulation, was achieved by the use of continuous computer-generated subwavelength dielectric gratings. However, applying the constraint on the continuity of the subwavelength grating led to spatial variations of the local period. As a result, the elements were restricted in their ability to form sophisticated phase functions, in addition to being limited in their physical dimensions. Moreover, the space-varying periodicity complicated the optimization of the photolithographic process. Recently, an approach which overcomes the limitations of the continuous design has been presented [13,14]. In this technique, the elements are formed by discretely controlling the local orientation of subwavelength grating while maintaining uniform periodicity. The resulting phase modulation is also discrete, thereby producing elements that are discrete space-variant dielectric subwavelength gratings (DSGs). It has been shown that approximating the desired phase with a sufficient number of discrete levels results in negligible diffraction from the phase discontinuities [13].

In this paper, we propose the formation of helical beams with different topological charges by use of DSGs. The elements were realized on GaAs wafers for circularly polarized CO_2 laser radiation with a wavelength of 10.6 μm. In Section 2, we describe how the geometrical phase that accompanies space-variant polarization state manipulation can be utilized to form helical phase distributions. Section 3 is devoted to the design and fabrication of elements with various topological charges. Experimental verification of their properties is given in Section 4. The verification was obtained by illuminating the elements with linearly polarized light, which produced self-interference of the emerging beam. Both the helical phase structure and the grating's birefringent parameters were determined by analyzing the resulting fringe patterns. The experiments showed that high quality helical beams were efficiently formed using thin, lightweight elements. Finally, concluding remarks are provided in Section 5.

2. Theory

DSGs can be considered as wave plates with constant retardation and a space-varying fast axis. It is convenient to form such space-varying wave plates using subwavelength gratings. When the period of grating is smaller than the incident wavelength, only the zero order is a propagating order and all other orders are evanescent. In this case, the grating behaves as a uniaxial crystal with the optical axes parallel and perpendicular to the subwavelength grooves [15–17]. Therefore, by fabricating a subwavelength grating for which the orientation of the subwavelength grooves is changed along the face of the element, a space-variant wave plate can be realized. Insight into the physical behavior of DSGs can be gained by performing polarization and phase analysis of the emerging beams. For this purpose, Jones calculus is a convenient means in the case of fully polarized incident waves. In this formalism, the space-invariant subwavelength grating is expressed by the matrix

$$\mathbf{J} = \begin{pmatrix} t_x & 0 \\ 0 & t_y e^{i\phi} \end{pmatrix}, \tag{1}$$

where t_x, t_y are the real amplitude transmission coefficients for light polarized perpendicular and parallel to the grating grooves and ϕ is the retardation of the grating. If the orientation of the subwavelength grooves is space-varying, then the transmission of the subwavelength structure can be described by the space-dependent matrix

$$\mathbf{T}(x,y) = \mathbf{M}^{-1}(\theta)\mathbf{J}\mathbf{M}(\theta), \tag{2}$$

where $\theta = \theta(x,y)$ is the local orientation of the subwavelength grooves and

$$\mathbf{M}(\theta) = \begin{pmatrix} \cos\theta & \sin\theta \\ -\sin\theta & \cos\theta \end{pmatrix} \tag{3}$$

is the two-dimensional rotation matrix. For convenience, we represent Jones vectors in the Dirac bra-ket notation. Let $|E_{in}\rangle$ denote the polarization state of a beam incident upon a DSG. Using Eq. (2), the emerging beam can be calculated as:

$$|E_{\text{out}}\rangle = \mathbf{T}|E_{\text{in}}\rangle = \frac{1}{2}(t_x + t_y e^{i\phi})|E_{\text{in}}\rangle + \frac{1}{2}(t_x - t_y e^{i\phi})\left[e^{i2\theta}|R\rangle\langle L|E_{\text{in}}\rangle + e^{-i2\theta}|L\rangle\langle R|E_{\text{in}}\rangle\right], \quad (4)$$

where $|R\rangle = (1,-i)^T/\sqrt{2}$ and $|L\rangle = (1,i)^T/\sqrt{2}$ are right- and left-handed circularly polarized unit vectors, respectively, and $\langle\alpha|\beta\rangle$ denotes the inner product. Eq. (4) indicates that the beam emerging from a DSG comprises three polarization orders. The first order maintains the original polarization and phase of the incoming beam. The second is a right-handed circularly polarized and has a phase modulation of $2\theta(x,y)$. The third order has an orthogonal polarization direction and an opposite phase modification with respect to the second order. Note that the magnitude of the different orders is determined by the local birefringent parameters t_x, t_y and ϕ as well as by the incoming polarization state, for the $|R\rangle$ and $|L\rangle$ orders. In the substantial case of $t_x = t_y = 1$ and $\phi = \pi$, an incident beam with $|R\rangle$ polarization is subject to total polarization state conversion that results in an emerging field of the form:

$$|E_{\text{out}}\rangle = e^{-i2\theta(x,y)}|L\rangle. \quad (5)$$

An important property of Eq. (5) is the phase factor $-2\theta(x,y)$, which depends solely on the local orientation of the grating grooves. This dependency is geometrical in nature and arises from spatial changes in the polarization state of the beam. It can be illustrated by use of the Poincaré sphere. This is a unit sphere for which the three normalized Stokes parameters S_1/S_0, S_2/S_0 and S_3/S_0 represent locations along the rectangular directions, as depicted in Fig. 1. The incident right-handed polarized beam and the transmitted left-handed polarized beams correspond to the north and south poles of the sphere, respectively. Inasmuch as the subwavelength grating is space-varying, the polarization state of the beam at different locations traverses different paths on the Poincaré sphere. For instance, the geodesic lines A and B represent different paths traversed by the polarization state of the beam when transmitted through element domains of local orientations $\theta(r,0)$ and $\theta(r,\omega)$, respectively. Geometrical calculations show that the phase difference acquired by the beam equals half of the area (shaded in the figure) enclosed by geodesic lines A and B on the sphere [14,18]. This fact is in compliance with the well-known rule proposed by Pancharatnam for comparing the phases of two light beams with different polarizations [19] and can be considered an extension of the rule into the space-domain. Note that from Eq. (4) it is obvious that for $|L\rangle$ illumination, the emerging beam is $|R\rangle$ polarized and its phase modulation is opposite in sign.

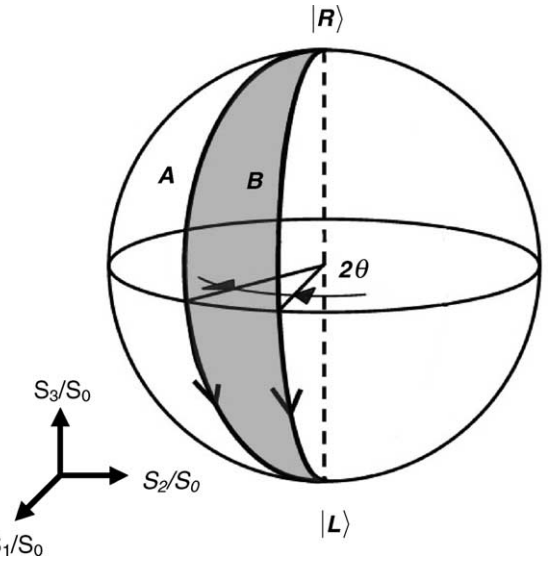

Fig. 1. Illustration of the principle of DSGs, using a Poincaré sphere. It shows the transformation from a right- to a left-handed circular polarization state as geodesic paths on the Poincaré sphere.

3. Design procedure and fabrication process

In our approach, a continuous desired phase function $\varphi_d(x,y)$ is approximated by discrete phase steps leading to discrete groove orientation. In compliance with Eq. (5), the connection between the desired phase and the discrete groove orientation is given by

$$\theta(x,y)|_{\text{mod}\pi} = -F_N(\varphi_d(x,y))/2, \quad (6)$$

where $F_N(\,)$ denotes a process that divides the desired phase, φ_d, into N equal levels. This division process is depicted in Fig. 2, where the actual

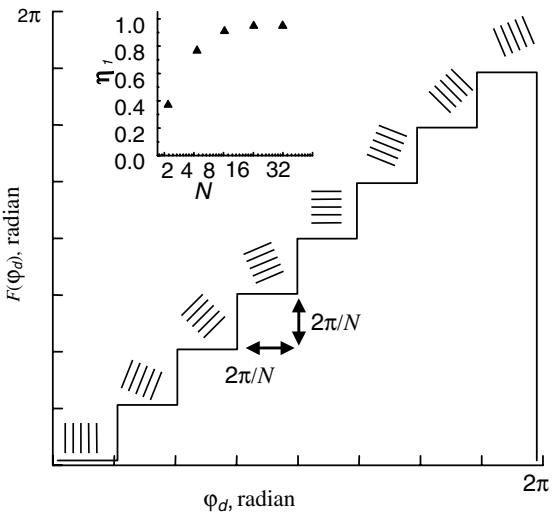

Fig. 2. Actual discrete phase $F_N(\varphi_d)$ as a function of the desired phase φ_d, along with the discrete local grating orientation. Inset shows the predicted first order diffraction efficiency as a function of the number of discrete levels N.

phase, $\varphi(x,y) = F(\varphi_d(x,y))$, is given as a function of the desired phase as well as the discrete local groove orientation. In the scalar approximation, an incident beam is multiplied by the phase function of the discrete phase element resulting in diffraction of the emerging beam. Quantification of this diffraction is obtained by Fourier expansion of the actual phase,

$$\exp(\mathrm{i}F_N(\varphi_d)) = \sum_m C_m \exp(\mathrm{i}m\varphi_d), \tag{7}$$

where C_m is the mth order coefficient of the Fourier expansion. The diffraction efficiency, η_m, of the mth diffracted order is given by $\eta_m = |C_m|^2$. The first diffraction order represents an exact replica of the desired phase φ_d. Consequently, the diffraction efficiency η_1 for the first diffracted order is related to the number of discrete levels N by

$$\eta_1 = \left[\frac{N}{\pi}\sin\left(\frac{\pi}{N}\right)\right]^2. \tag{8}$$

This equation indicates that for 2, 4, 8, and 16 discrete phase levels, the diffraction efficiency will be 40.5%, 81.1%, 95.0%, and 98.7%, respectively. This connection between the first order diffraction efficiency and the number of discrete levels is also given in Fig. 2 and was verified experimentally in [13].

Our objective was to design an element that when illuminated with $|R\rangle$ polarized beam produced a helical phase distribution. Such an element can be obtained by requiring that

$$\varphi_d = l\omega, \tag{9}$$

and by using Eq. (6) to determine the local subwavelength grating groove orientation. We realized binary chrome masks for $l = 1$, 2, 3 and 4 by using high-resolution laser lithography. The amplitude transmission, $t(x,y)$, of the masks is derived from

$$t(x,y) = U_\mathrm{s}\left[\cos\left(\frac{2\pi}{\Lambda}(x\cos\theta(x,y) + y\sin\theta(x,y))\right) - \cos(\pi q)\right], \tag{10}$$

where Λ and q are the period and fill factor of the subwavelength grating, respectively, and U_s is the unit step function defined by

$$U_\mathrm{s}(\xi) = \begin{cases} 1, & \xi \geqslant 0, \\ 0, & \xi < 0. \end{cases} \tag{11}$$

The masks were 10 mm in diameter and $\theta(x,y)$ was found from Eq. (6) with a number of discrete levels $N = 16$. According to Eq. (8), we expect more than a 98% diffraction efficiency into the first order. A subwavelength period of $\Lambda = 2$ μm was selected together with a fill factor $q = 0.5$ for use with CO_2 laser radiation with a 10.6 μm wavelength. Fig. 3 shows magnified

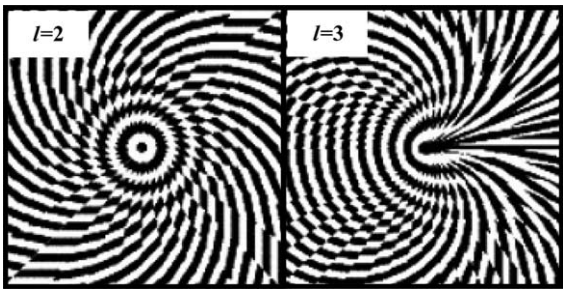

Fig. 3. Magnified geometries of the masks for topological charges $l = 2, 3$.

geometries of the masks for topological charges 2 and 3. The masks were transferred by contact lithography to 500 μm thick GaAs wafers that were pre-deposited with a 2000 Å layer of SiN_x. The SiN_x deposition was achieved by enhanced chemical vapor deposition (PECVD) at 900 mTorr and 300 °C. At this stage, a 700 Å Ni adhesion layer was used for the lift-off process. Next, the SiN_x layer was etched through the Ni strips, which served as a mask. The etching was performed by reactive ion etching (RIE) for 30 s at room temperature with CF_4 and O_2 at gas flow rates of 35 and 14 sccm, respectively, and at a pressure of 80 mTorr. The GaAs was etched by electron cyclone resonance (ECR) for about four minutes, with the etched SiN_x layer serving as a mask. The ECR conditions were: 20 sccm of Cl_2, 5 sccm of Ar, 75 W RF power and 600 W microwave power, at 100 °C. The remaining SiN_x was removed using HF acid resulting in a grating of 5 μm nominal depth. At this stage, an anti-reflection coating was deposited on the backside of the element to finish the fabrication of the desired DSG. Fig. 4(a) shows a scanning electron microscope (SEM) image of the central part of the $l = 3$ element. The area in the center of the element where the pattern is distorted is about 10 μm in diameter, and therefore can be disregarded. Fig. 4(b) shows a SEM image of the subwavelength grooves for $l = 4$. Note the high aspect ratio (~1/5) and the rectangular shape of the grooves.

4. Experimental results

The actual phase distribution, φ, as well as the actual local birefringent parameters t_x, t_y and ϕ were determined based on the fact that the transmission of the DSG is polarization dependent. From Eq. (4) it is evident that when a DSG is illuminated with linearly polarized light, the emerging beam is the coherent sum of at least two of the polarization orders. By imaging the beam through a quarter wave plate followed by a linear polarizer at different orientations, self-interference of the polarization orders is obtained. Different combinations of quarter wave plate and polarizer orientations yield different fringe patterns. These fringe patterns contain information about the phase structure of the beam and the birefringent parameters of the elements. However, as a Jones vector contains three independent parameters (the two amplitudes and the phase retardation between them), it is not possible to obtain more than three independent parameters from a single illumination. In our case, the elements were illuminated with horizontally linear polarized light and with right-handed circularly polarized light. The Stokes parameters were used to express the measured quantities [20]. Although this choice yields an overly determinant set of equations, the calculation itself becomes simpler. In terms of circular polarizations, the Stokes parameters of a monochromatic beam are given by

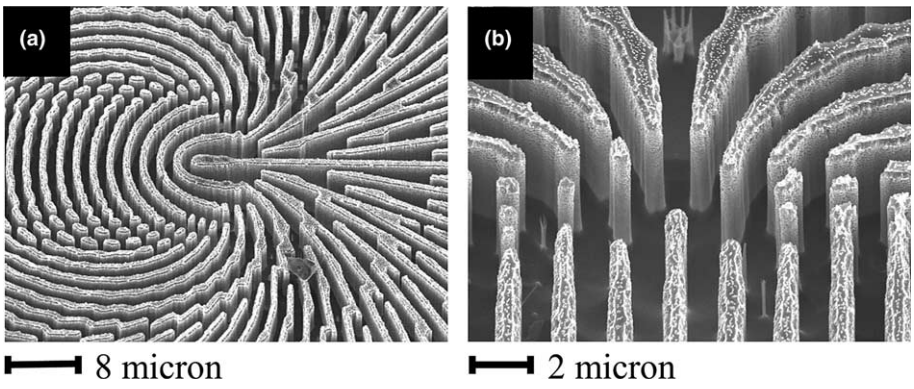

Fig. 4. Scanning electron microscope images of the central parts of the elements having topological charge (a) $l = 3$, and (b) $l = 4$.

$$\begin{aligned} S_0 &= |\langle R|E\rangle|^2 + |\langle L|E\rangle|^2, \\ S_1 &= \langle R|E\rangle\langle E|L\rangle + \langle L|E\rangle\langle E|R\rangle, \\ S_2 &= -\mathrm{i}(\langle R|E\rangle\langle E|L\rangle - \langle L|E\rangle\langle E|R\rangle), \\ S_3 &= |\langle L|E\rangle|^2 - |\langle R|E\rangle|^2. \end{aligned} \tag{12}$$

In the most general case, the Jones vectors of the beams beyond the element for the two illuminations are given by Eq. (4). These Jones vectors are then used with Eq. (12) to obtain the Stokes parameters immediately behind the element. In the case of horizontally linear illumination, we find

$$\begin{aligned} S_0^{\mathrm{H}} &= \frac{A}{2} + \frac{B}{2}\cos(\varphi), \\ S_1^{\mathrm{H}} &= \frac{A}{4} + \frac{C}{2}\cos(\phi) + \frac{B}{2}\cos(\varphi) \\ &\quad + \left(\frac{A}{4} - \frac{C}{2}\cos(\phi)\right)\cos(2\varphi), \\ S_2^{\mathrm{H}} &= \frac{B}{2}\sin(\varphi) + \left(\frac{A}{4} - \frac{C}{2}\cos(\phi)\right)\sin(2\varphi), \\ S_3^{\mathrm{H}} &= -C\sin(\phi)\sin(\varphi), \end{aligned} \tag{13}$$

where $A = t_x^2 + t_y^2$, $B = t_x^2 - t_y^2$, and $C = t_x t_y$. For the right-handed circularly polarized illumination, the Stokes parameters are given by

$$\begin{aligned} S_0^{\mathrm{R}} &= \frac{A}{2}, \\ S_1^{\mathrm{R}} &= \frac{1}{2}[B\cos(\varphi) - 2C\sin(\phi)\sin(\varphi)], \\ S_2^{\mathrm{R}} &= \frac{1}{2}[B\sin(\varphi) + 2C\sin(\phi)\cos(\varphi)], \\ S_3^{\mathrm{R}} &= -C\sin(\phi). \end{aligned} \tag{14}$$

The terms depending on twice the actual phase, φ, are dominant in Eq. (13), in the current case of interest ($t_x \approx t_y \approx 1, \phi \approx \pi$). We therefore find, by use of Eqs. (13) and (14),

$$\cos(2\varphi) = 1 - 2\frac{S_0^{\mathrm{H}} - S_1^{\mathrm{H}}}{S_0^{\mathrm{R}} + S_3^{\mathrm{R}}}. \tag{15}$$

The parameters A and B are found from

$$A = 2S_0^{\mathrm{R}}, \quad B = \frac{2S_0^{\mathrm{H}} - A}{\cos(\varphi)}. \tag{16}$$

We avoid an explicit calculation of φ by using the well-known trigonometric identity, $\cos(\varphi) = \sqrt{(1+\cos(2\varphi))/2}$. Moreover, the birefringent parameters are found from

$$t_x = \sqrt{\frac{A+B}{2}}, \quad t_y = \sqrt{\frac{A-B}{2}}, \quad \cos(\phi) = \frac{-2S_3^{\mathrm{R}}}{\sqrt{A^2 - B^2}}. \tag{17}$$

Eqs. (15)–(17) enable simple measurement of the phase modification and the birefringent parameters of a DSG. The measurements were carried out by illuminating the DSG with suitably prepared CO_2 laser radiation. The emerging beams were imaged onto a two-dimensional pyroelectric detection array (Spiricon Pyrocam III camera) through a quarter wave plate followed by a polarizer. The Stokes parameters for the different illuminations were calculated from the measured intensities by the following expressions:

$$\begin{aligned} S_0 &= I_{45,0} + I_{-45,0}, \\ S_1 &= 2I_{0,0} - S_0, \\ S_2 &= 2I_{45,45} - S_0, \\ S_3 &= I_{45,0} - I_{-45,0}, \end{aligned} \tag{18}$$

where $I_{\alpha,\beta}$ represents the measured intensity obtained with the quarter wave plate oriented at an angle α followed by a polarizer oriented at an angle β. In addition, the measurements were normalized by the incoming intensity in order to prevent non-uniformity of the incoming beam from affecting the results. This method for obtaining the Stokes parameters is known as the four-measurement technique [21]. Fig. 5 shows the experimental results of $I_{45,45}$ and $I_{45,0}$ for horizontally linear polarized illumination as well as S_1^{H} by use of Eq. (18). The fringes demonstrate the self-interference of the emerging beam. The $I_{45,0}$ term corresponds to the amount of the left-handed circular polarization within the emerging beam. In the ideal case, for which $t_x = t_y = 1$ and $\phi = \pi$, this term becomes uniformly distributed as evident from Eq. (4). Therefore, the modulation observed in Fig. 5(b) is a result of the imperfections in t_x, t_y and ϕ, indicating the existence of the first polarization order. The measured phase distribution, obtained from Eq. (15), for beam with topological charge 1 is shown in Fig. 5(d). The typical standard deviation (STD) of the phase fronts from their desired

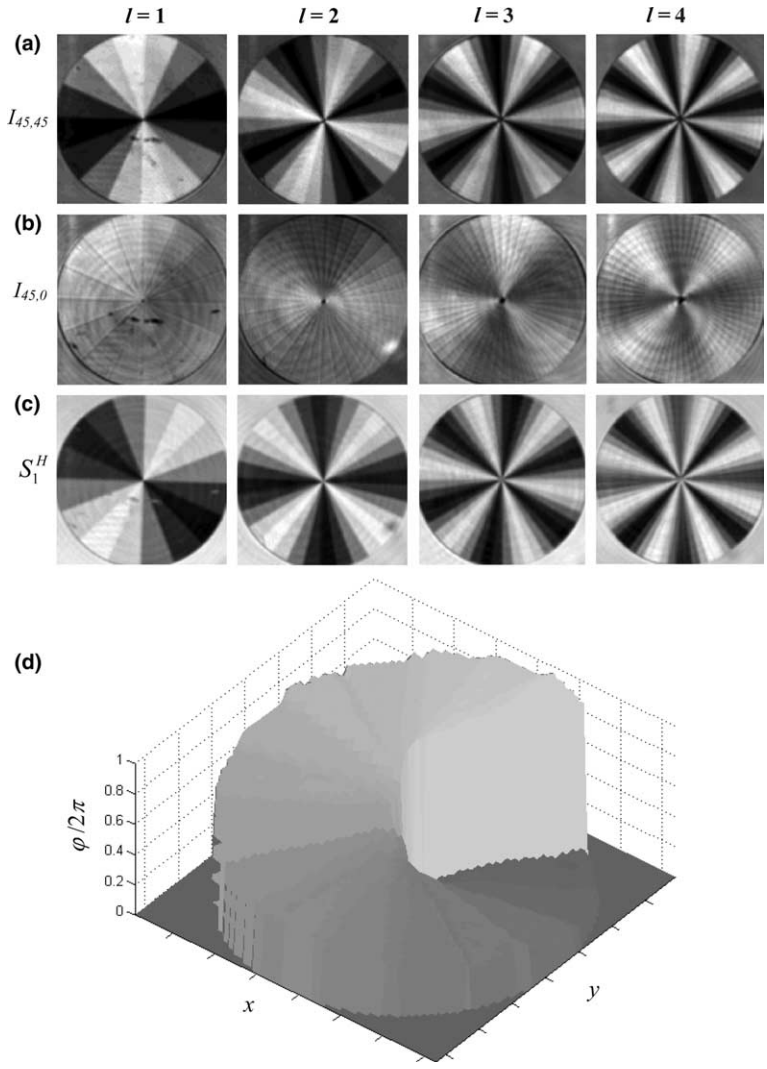

Fig. 5. The experimental self-interference patterns obtained for horizontally linear polarized illumination of DSGs with $l = 1$–4, with a quarter wave plate oriented at 45° and a polarizer oriented at 45° in (a) and 0° in (b). The measured S_1^H is shown in (c). (d) The measured phase distribution of the beam with $l = 1$.

value was 2.5%, indicating that high quality spiral phase distributions had been formed. For the local grating coefficients, t_x, t_y and ϕ, typical values of 0.86, 0.74 and 0.97π with STD of about 10% were obtained, respectively, by use of Eqs. (16) and (17). These values are close to the theoretical predictions achieved by a rigorous coupled-wave analysis utilizing the measured profiles of the gratings.

Sometimes, the far-field image of the helical beam is the desired feature. This far-field is characterized by a doughnut-shaped intensity pattern that results from the phase singularity at the center of the beam. In Fig. 6 the far-field intensity patterns for the various topological charges are presented. The images were obtained at the focus of a 500 mm focal length lens. Also shown in Fig. 6 are the typical cross-sections and the corresponding theoretical predictions. Note that for the higher topological charges, a deviation from the theoretical prediction appears as a bright central spot. We measured this bright spot to be orthogo-

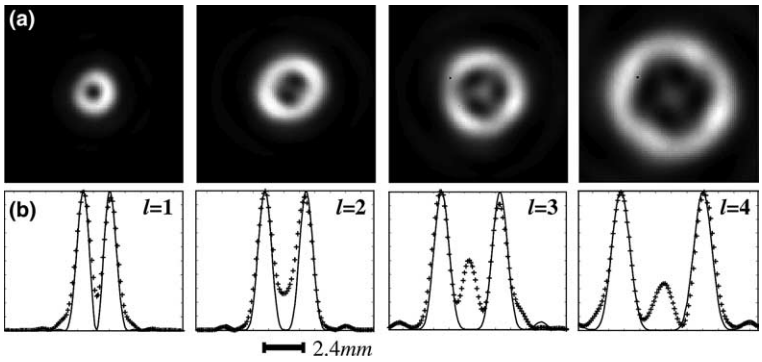

Fig. 6. Experimental far-field images (a), and their calculated (solid lines) and measured (crosses) cross-sections (b), for the helical beams with $l = 1$–4 emerging from the DSGs for right-handed circular polarized illumination.

nally polarized with respect to the doughnut-shaped intensity. This indicates that the central spot can be attributed to the first polarization order of Eq. (4). Using the measured values for t_x, t_y and ϕ we calculated this residual intensity to be 0.85% of the overall transmitted intensity. We measured the central spot intensity as 1% of the overall intensity, in agreement with our predictions. The central spot can be easily removed by transmitting the beams through a suitably prepared circular polarizer. A circular polarizer is an apparatus composed of a quarter wave plate oriented at ±45° followed by a linear polarizer at 0°. The orientation of the plate determines whether a left- or right-handed circular polarization is transmitted by the apparatus. Fig. 7 shows the measured intensity patterns and cross-sections for the beams transmitted through a circular polarizer designed to transmit left-handed circularly polarized light. Also note in Fig. 6 that the intensity pattern for $l = 2$ is somewhat elongated, for $l = 3$ it is somewhat triangular and for $l = 4$ the intensity pattern is somewhat of rectangular shape. This is due to some anisotropic behavior of the etching process that resulted in systematic changes in the grating parameters. These imperfections are partially removed by the circular polarizer, as can be seen from the relatively symmetric and uniform doughnut-shaped images of Fig. 7.

Actually, the geometrical phase modification is determined by the space-variant groove orientation. Therefore, the optical quality of the hybrid element, composed of a DSG and a circular polarizer, is mainly determined by the extinction ratio

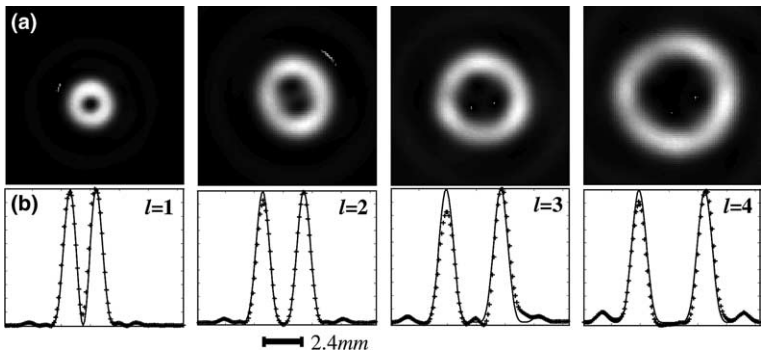

Fig. 7. Experimental far-field images (a), and their calculated (solid lines) and measured (crosses) cross-sections (b), for the helical beams with $l = 1$–4 emerging from the DSGs for right-handed circular polarized illumination. The emerging beams were transmitted through a left-handed circular polarizer.

of the circular polarizer as well as the number of discrete levels N. The difficulty in accurately controlling the groove shape by use of the lithographic process merely determines the overall transmission of the element. This is due to the dependency of the birefringent parameters, t_x, t_y and ϕ, on the profile of the grooves. Consequently, from Eq. (4) we find that the deviation in the desired parameters ($t_x = t_y = 1$ and $\phi = \pi$) results in intensity transfer from the desired polarization order into the first polarization order. The experimental errors in the birefringent parameters have no effect on the phase of the desired polarization and we have demonstrated in the experiment that the circular polarizer can be used to remove any residual intensity.

5. Conclusions

To conclude, we have demonstrated that spiral phase elements can be realized by computer-generated space-variant subwavelength gratings. The elements are thin, lightweight and highly efficient. The derived phase of the DSG was not a result of optical path differences, but solely due to local changes in polarization, which was in fact, a manifestation of the geometrical space-domain Pancharatnam phase. Several advantages were found in using DSGs over conventional kinoform diffractive optical elements or refractive optics. The phase modification of a DSG depends only on the local orientation of the subwavelength grooves rather than on the groove's shape and depth. In a standard lithographic process, the groove orientation is a fairly robust quantity, while the three-dimensional profile of the grooves is highly sensitive to the specific process applied. Therefore, by use of DSGs, it enables to obtain accurate complex phases with a single mask process, and ensures high repeatability of optical performance. Also, a hybrid element composed of a DSG and a circular polarizer yields an achromatic phase element, although with some intensity loss for wavelengths different from the nominal value [22]. This intensity loss is due to the wavelength dependency of the birefringent parameters. Furthermore, DSGs are polarization-dependent and thus enables to obtain multipurpose elements [23]. Finally, the use of standard lithographic processes makes the elements inherently suitable for the large-scale integration of optical components.

References

[1] L. Allen, M.J. Padgett, M. Babiker, in: E. Wolf (Ed.), Progress in Optics, vol. 39, North-Holland, Amsterdam, 1999.
[2] K.T. Gahagan, G.A. Swartzlander Jr., Opt. Lett. 21 (1996) 827.
[3] N.B. Simpson, K. Dholakia, L. Allen, M.J. Padgett, Opt. Lett. 22 (1997) 52.
[4] L. Paterson, M.P. MacDonald, J. Arlt, W. Sibbett, P.E. Bryant, K. Dholakia, Science 292 (2001) 912.
[5] V. Garcés-Chávez, D. McGloin, H. Melville, W. Sibbett, K. Dholakia, Nature 419 (2002) 145.
[6] S.N. Khonina, V.V. Kotlyar, M.V. Shinkaryev, V.A. Soifer, G.V. Uspleniev, J. Mod. Opt. 39 (1992) 1147.
[7] J. Courtial, D.A. Robertson, K. Dholakia, L. Allen, M.J. Padgett, Phys. Rev. Lett. 81 (1998) 4828.
[8] Z.S. Sacks, D. Rozas, G.A. Swartzlander Jr., J. Opt. Soc. Am. B 15 (1998) 2226.
[9] Q. Wang, X.W. Sun, P. Shum, Appl. Opt. 43 (2004) 2292.
[10] M.W. Beijersbergen, R.P.C. Coerwinkel, M. Kristensen, J.P. Woerdman, Opt. Commun. 112 (1994) 321.
[11] R. Oron, N. Davidson, A.A. Friesem, E. Hasman, in: E. Wolf (Ed.), Progress in Optics, vol. 42, North-Holland, Amsterdam, 2001.
[12] G. Biener, A. Niv, V. Kleiner, E. Hasman, Opt. Lett. 27 (2002) 1875.
[13] E. Hasman, V. Kleiner, G. Biener, A. Niv, Appl. Phys. Lett. 82 (2003) 328.
[14] E. Hasman, G. Biener, A. Niv, V. Kleiner, in: E. Wolf (Ed.), Progress in Optics, vol. 47, North-Holland, Amsterdam, 2005.
[15] M. Born, E. Wolf, Principles of Optics, seventh ed., Cambridge University Press, Cambridge, UK, 1999 (Section. 15.5.2).
[16] R.C. Enger, S.K. Case, Appl. Opt. 22 (1983) 3220.
[17] L.H. Cescato, E. Gluch, N. Streibl, Appl. Opt. 29 (1990) 3286.
[18] Z. Bomzon, V. Kleiner, E. Hasman, Opt. Lett. 26 (2001) 1424.
[19] S. Pancharatnam, Proc. Ind. Acad. Sci. A 44 (1956) 247 (reprinted in S. Pancharatnam, Collected Works, Oxford University Press, 1975).
[20] C. Brosseau, Fundamentals of Polarized Light, Wiley, New York, 1998.
[21] E. Collet, Polarized Light, Marcel Dekker, New York, 1993.
[22] H. Lajunen, J. Tervo, J. Turunen, Opt. Lett. 29 (2004) 803.
[23] E. Hasman, Z. Bomzon, A. Niv, G. Biener, V. Kleiner, Opt. Commun. 209 (2002) 45.